2017

Manipulating Lipid Spreading Domain Formation with Compositional Gradients and Plasmonic Nanoparticles

Chen-min Hung
Claremont McKenna College

Manipulating lipid spreading domain formation with compositional gradients and plasmonic nanoparticles

A Thesis Presented

by

Chen-min (Steven) Hung

To the Keck Science Department

Of Claremont McKenna, Pitzer, and Scripps Collges

In partial fulfillment of

The degree of Bachelor of Arts

Senior Thesis in Chemistry

December 6, 2016

Contents

Abstract

After colliding two solid-supported spreading bilayers of different compositions, we produce a dynamic gradient as the newly-healed bilayer equilibrates. We apply this approach to study the formation of galactosyl ceramide (GalCer) domains. With a single experiment, we are able to explore the effects of varying cholesterol concentration on GalCer domains. To further control domain formation, we aimed to locally heat membranes with embedded plasmonic nanoparticles. However, we discovered a percolation threshold of spreading lipids over the array of nanoparticles. We found that surfaces with gold nanoparticles deposited at an average inter-particle distance of 40 nm inhibited lipid bilayer spreading, but the same bilayer was able to spread onto similar surfaces with a sparser array of nanoparticles.

Chapter 1

Introduction and Historical Background

1.1 Lipid bilayer membrane

1.1.1 Relevance in biological environment

A lipid bilayer membrane is one essential ingredient to the origin of life. As a barrier, it separates the inside of a cell from the outside, and while nonpolar molecules can freely diffuse through the membrane, most other bigger, polar, or charged molecules do not have free passage unless there is a specially-designated pathway or channel that allows the molecule to travel through [1]. In the primordial soup theory for the origin of life, the formation of fatty acids, possibly at the hydrothermal vents, and their subsequent aggregation and self-assembly into leaflets of lipid bilayer and finally vesicles provided an enclosed space for RNA replicases to efficiently replicate and prosper [2]. In the same way, the lipid bilayer membrane may have helped the early cell retain life-supporting molecules inside the cell and the harmful or unnecessary molecules outside the cell, and to this day they continue to provide this function to most organisms on planet earth [2].

Fatty acids and phospholipids are amphipathic compounds that have a hydrophilic

head group connected to a hydrophobic chain of hydrocarbons. On the molecular level, the long hydrophobic alkyl chains present an unfavorable situation in water where water molecules surrounding the alkyl chain are restricted from their typical rotational and vibrational freedom. This unfavorable situation induces the hydrophobic effect, where lipids and other nonpolar molecules cluster together over time so that the total area of unfavorable interactions with water molecules is reduced [3]. With their polar head groups, fatty acids and phospholipids can form even more energetically favorable micelles and bilayers as the hydrophobic chains cluster together and hydrophilic heads cluster together. A vesicle is further formed when a bilayer folds on itself, and an inner water-based compartment is created for storage of materials [4].

According to the theory of evolution, over the billions of years of life variations were constantly introduced into membranes and some advantageous features were conserved. Fatty acids were replaced by phospholipids with specific head groups and specific hydrocarbon tails, some completely saturated and some with kinks of unsaturation. Proteins, sugars, and other lipids inserted themselves into specific leaflets and regions of the bilayer membrane to provide important functions including transport, signal transduction, cell-cell adhesion and more. Membranes also serve important functions in intracellular organelles for purposes such as energy production and nutrients storage. In order to achieve a "satisfactory" understanding of how biological membranes function, Singer and Nicolson set out to study the molecular composition and structure of membranes [5]; in 1972, Singer and Nicolson proposed the Fluid-Mosaic Model to describe biological membranes as "a two-dimensional solution of integral proteins (lipoproteins) in the viscous phospholipid bilayer solvent" [6] based on thermodynamic analysis of experimental data. Research on membranes continues to progress over the years, and in a 2014 update of the model, Nicolson emphasized the role of membrane macrostructures such as lipid rafts and protein complexes in restraining the rotational and lateral motilities of membrane components – the mosaic nature of the model [5].

1.1.2 The supported lipid bilayer model

In an effort to study immune recognition, McConnell et al pioneered the supported lipid bilayer (SLB) model in 1984 in which they laid down lipid bilayer incorporated with H-2K^K protein on glass surfaces to observe the binding of antigens [7]. This practical method soon caught on to the rest of membrane research community. Adhered to a planar support, a supported lipid bilayer is two-dimensional and thus easier to observe and measure than their curved counterpart on vesicles [8]; with the addition of a small amount of fluorescently-labeled lipid, the supported bilayer can be readily observed by fluorescence microscopy [8]. Perhaps the most attractive characteristic of the model is that even though the bilayer lies on the solid support, the lower leaflet is not directly-attached to the solid support but instead separated by an ultrathin layer of water of approximately 10 Å thick, as confirmed by neutron scattering and NMR [9] ; the advantage of this separation allows lipid molecules the same Brownian level of fluidity as they are in vesicles or living cells [10]. Combining the benefits of observability and natural fluidity, the supported lipid bilayer model became an excellent platform to investigate "lipid domain formation, intermembrane interactions, or mechanical processes such as protein adsorption, protein self-assembly, protein localization at lipid boundaries, or protein functions."[11] Furthermore, techniques such as Fourier transform infrared spectroscopy (FTIR), nuclear magnetic resonance (NMR), total internal reflection fluorescence (TIRF), lateral diffusion measurements, ellipsometry can be employed to study the dynamic and structural properties of these bilayers [12].

Another useful property of the SLB is its ability to self-heal; just like vesicles can perform endocytosis by merging its bilayer into a living membrane, a similar fusing phenomenon takes place when two bilayers on supported substrate meet. The Rädler and Boxer groups conducted a series of experiments in the late 1990s to prove that this was true. Rädler's group put pinning obstacles in the path of an advancing line of lipid bilayer and observed that the bilayer circumvents the pins to grow back on itself, instead

of abruptly forcing a depinning action [13]. For the Rädler group, this observation started the idea of a "self-healing" membrane, as they conducted another experiment observing two advancing lipid fronts fuse into one another [13]. The Boxer group demonstrated similar findings by mechanically scratching a phospholipid bilayer and observing it self-heal in action [9], as well as peeling off an area of bilayer by exposure to air-water interface and observing the remaining bilayer grow back into the peeled-off region once it was re-hydrated [9]. Boxer concluded these experiments with the observation that as long as lipid reservoir is available, a bilayer would continue to spread and self-heal, but once the reservoir runs out, a bilayer would stop where it is [8].

1.1.3 Early preparation methods

By the early 1990s, there had been two common methods to prepare supported lipid bilayers [14, 15]. One method was the Langmuir-Blodgett technique which consecutively transfers two lipid monolayers onto a surface. The other was the vesicle fusion technique, which sonicates lipids to make lipid vesicles, adheres them onto a hydrophilic surface, and ruptures them . However, as research progresses, scientists became interested in experimental specifications that these two methods alone could not suffice. For example, with the Langmuir-Blodgett technique, Kalb et al. (1992) had difficulty incorporating proteins through the Langmuir trough as the bilayer was laid out in monolayers [14]. With the vesicle fusion technique, problems with vesicles not adhering to substrate or not entirely rupturing were encountered [13]. At the same time, research had been compiling to understand the physical properties of SLBs, one of which is spreading [16].

1.1.4 The stamp spreading method

The spreading phenomenon of phospholipid bilayer membrane was analogous to liquid wetting a solid surface that continues to spread as long as it is energetically favorable [16]. In 1995, Rädler et al. discovered this by depositing a lump of lipid onto a clean surface

and immersing it in aqueous environment, after which they observed lipid spreading out over the bare surface. Because of the aqueous environment, it was assumed that phospholipid spread out in the bilayer form to minimize unfavorable interactions. Rädler et al. proposed two mechanisms for this phenomenon: (i) Sliding of bilayer "on a thin lubricating water film" and (ii) the rolling over of the distal leaflet in a "tank tread type motion" [16]. A later study tracked photo-bleached particles on both leaflets as the bilayer spread and found that hydration-induced lipid bilayer spreading is predominantly the latter mechanism proposed by Rädler et al.—that the majority of the "slip" that takes place in spreading happens between the upper and lower leaflet, instead of between the lower leaflet and the substrate [17].

1.1.5 Applications of colliding spreading bilayers

An application of the stamp spreading method, in combination with the self-healing property, is to spread multiple stacks of phospholipids in close proximity to each other. As the lipid fronts collide and self-heal into one membrane, individual lipid molecules are allowed to laterally diffuse into areas previously dominated by lipids of the original stack source. Eventually, the molecules of the differing stacks should be uniformly dispersed over the entire area of the membrane. This project, however, capitalizes on the equilibrating process before complete diffusion is achieved. As molecules from different sources of the membrane begin to mix, a gradient forms in the region in between the stack sources. By colliding the appropriate combinations of stack components and lipid dyes, we have been able to figure out the diffusion coefficient of a POPC bilayer as well as a biotin-streptavidin binding curve with this gradient platform [18]. This study now seeks to further utilize this gradient platform to study phase separation behaviors in SLBs.

1.2 Lipid domains

An artificial bilayer model, such as the SLB, may appear stable and organized, but *in vivo* biological membranes are much more complicated, with a variety of components held together in different ways to accommodate for the range of functions required by the organism. Researchers have been utilizing the simplicity of SLBs to gain a better understanding of the various structures in a membrane.

1.2.1 Physical properties

Lipid domains are considered areas in a bilayer where same molecules cluster tightly together and become less fluid than the surrounding lipids; because identical molecules pack so tightly, lipid domains often exclude the bulky fluorescent labels incorporated in the bilayer and appear as dark shape in fluorescent microscopy [19]. One reason for this heterogeneity is the different composition of hydrophobic chain of the lipids. An unsaturation (a double bond) in a hydrocarbon chain introduces a rigid "kink" in the part of the tail where the *cis*-double bond is located; the presence of one or more unsaturated fatty acids in a membrane prohibits the molecules from packing as tightly as they would if all hydrocarbon chains were saturated. In this way, unsaturated fatty acids makes a membrane more fluid and have lower melting temperature; in fact, at physiological temperature (37°C), most saturated fatty acids exist in solid phase while most unsaturated acids exist in liquid phase [20].

In a lipid membrane, the phases of material are divided slightly differently into a semi-solid gel phase, a liquid-disordered state, and a liquid-ordered state. In the gel phase, all individual molecule motions are "strongly constrained; the bilayer is paracrystalline" [10]. In the liquid-disordered state, bilayer is very fluid and like a "sea of constantly moving lipids", and the liquid-ordered state is an intermediate between the gel and liquid-disordered phase, where molecular lateral fluidity is allowed but less favored [10].

Lipid domains form when there is a coexistence of different lipid states in one membrane. For example, on the outer leaflet of a cell plasma membrane, glycosphingolipids such as cerebrosides and gangliosides, which typically contain long, saturated fatty acids, form clusters that exclude glycerophospholipids such as phosphatidylcholines, which usually contain one unsaturated and one saturated acyl tail [10].

1.2.2 Biological relevance

The fraction of the typical cell membrane that exists in raft was estimated by the proportion of the plasma membrane that resists detergent solubilization, and it was found that as high as 50% of the cell surface was covered by rafts [10]. This explains why in the updated version of the Fluid-Mosaic Model, Nicolson now put more emphasis on the "mosaic nature of the macrostructure of cellular membranes" [5]. Lipid domains or lipid rafts play key roles in biological membranes, from hosting integral membranes to acting as membrane-associated cytoskeletal fences which limit lateral diffusion and range of motion of membrane components [5].

Galactosyl ceramide (GalCer), a sphingolipid with the sugar galactose, is a good case in point for this discussion. Known as an alternative receptor for the HIV envelope protein gp120 [21, 22] and a key player in the activation of T-cell activation [23, 24], GalCer is a biologically significant lipid whose physical property in the membrane is valuable to study. In 2007, Lin et al. conducted an extensive study on GalCer phase behavior over a range of cholesterol concentration in coexistence with phosphatidylcholines of different degrees of unsaturation [25]. This thesis intends to employ the gradient platform of colliding lipid bilayers to confirm a few findings Lin et al had about 1-palmitoyl-2-oleoyl-*sn*-glycerol-3-phosphocholine (POPC), GalCer, and cholesterol.

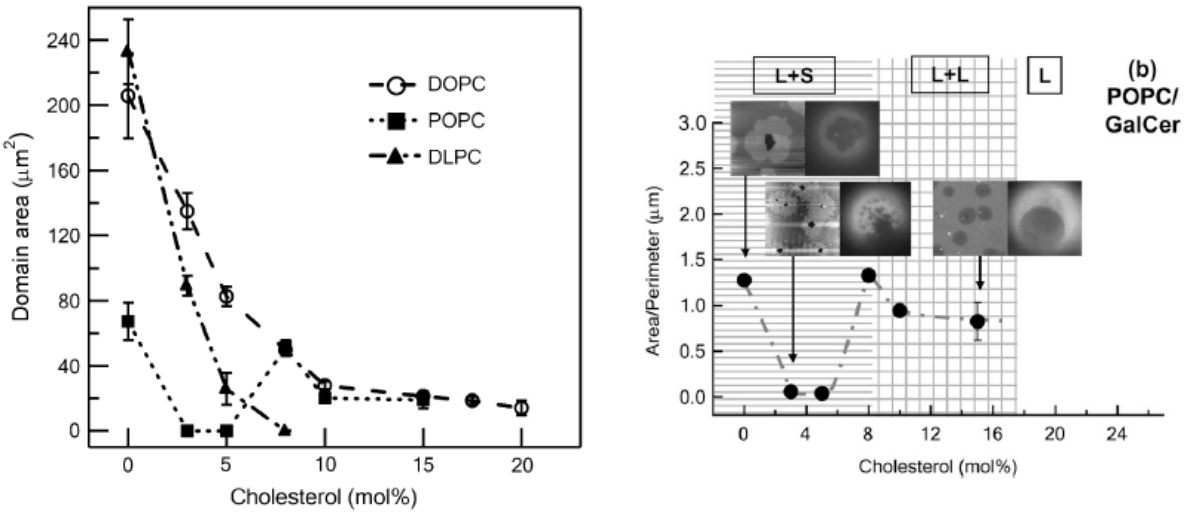

Figure 1.1: Figures 2 and 3b from *Fluid-Phase Chain Unsaturation Controlling Domain Microstructure and Phase in Ternary Lipid Bilayers Containing GalCer and Cholesterol* by Lin et al. (2007) [25]. On the left, SLB GalCer domain areas in POPC bilayers were tracked by black squares across mole fractions. On the right, area/perimeter ratio was recorded, and GalCer domain were compared across the SLB and giant unilamellar vesicles (GUV) formats. In addition, it was observed that bilayer and domain coexisted as liquid-solid from 0 to 8% cholesterol and as liquid disordered-liquid ordered from 10% to 14% cholesterol.

1.2.3 Research on formation components

Lin et al (2007) made POPC-based (65%) solid-supported bilayers that incorporate a combined 35% concentration of GalCer and cholesterol; they varied cholesterol concentration from 0% to 15% and GalCer concentration from 35% to 20% and used atomic force microscopy (AFM) to measure the area, the area/perimeter ratio, and height of GalCer domains. They found that at 0% and 8% cholesterol, GalCer domains appear similar in shape and size, but in between at 3% and 5%, individual domain areas reduce from micro-scale to nano-scale in size (see Figure 1.1) [25].

1.2.4 The role of slow-cooling in domain formation

With the stamp spreading method, lipids spread out from source as a homogeneous bilayer despite composing domain-forming lipids. Szmodis et al. (2010) manipulated

GalCer domain formation and meltage by adjusting temperature above and below the GalCer melting point. Furthermore, they found that slow-cooling at a rate of 0.07°C/min induces domains to grow to an average size of 700 μm^2, as opposed to the other mode observed at 100 μm^2 on average [26]. These big domains have fractal-like features, and Szmodis et al. attribute the large size and dendritic shape to the high GalCer-GalCer interaction energy that is allowed enough time to act in the slow-cooling time-frame. They suggested that the force of gel-fluid interfacial line tension is insufficient to restrict domain growth during the slow-cooling process, but as membrane equilibrates over an extended period, line tension does play a role in reshaping domains to be more circular [26].

1.2.5 Role of cholesterol in domains

Cholesterol exhibits stronger interactions with saturated fatty acids, as Lin et al. demonstrated decreasing cholesterol interaction from DLPC (two saturated acyl chains) to POPC (one saturated and one unsaturated acyl chain) to DOPC (two unsaturated acyl chains) [25]. To reduce complexity, this thesis considers solely conditions involving POPC. When inserted into a membrane, cholesterol's rigid planar structure reduces the rotational freedom of neighboring side chains, forcing them to into their fully extended conformation. Surrounded lipids tend to be in liquid-ordered phase, and because their acyl chains are fully extended, the leaflet becomes thicker [10].

1.3 Domain Heating with gold nanoparticles

Gold nanoparticles have been shown to be able to very efficiently convert light to heat. Especially at the corresponding plasmon wavelength, light-to-heat conversion has been found to be almost 1 [27]. Biomimetics has already taken advantage of this property as a number of studies have embedded gold nanoparticles in lipid bilayers as a source of

localized heating [28]. This heating application has been used to melt lipid domains [28, 29] as well as alter current across a membrane [30]. Overall, users have found the heating application dynamic as temperature and effect-area can be deliberately adjusted by power of light source and size of nanoparticles [28–30]. We envision embedding the same nanoparticles application into our gradient platform to locally manipulate temperature, so as to engineer more modes of composition gradients as temperature control induces localized phase transitions.

1.4 Percolation threshold

Experimentally, as we were creating a bilayer membrane surface with embedded gold nanoparticles, we encountered a problem that may be associated with pinning. Originally, we attempted to spread lipids into a glass area that has been deposited with gold nanoparticles (10 nm in diameter) at such density that the average interparticle distance was around 40 nm; the stack of lipid did not spread out as it usually did on a plasma-treated glass surface. Later, we spread lipid into an area deposited with gold nanoparticles at a lower density (average interparticle distance was estimated to be 100 nm), and the stack of lipid was able to spread as it normally does.

1.4.1 Theory

Nissen et al. (1999) observed that in the case of lipid spreading or any wetting phenomenon, the medium in concern was a two-dimensional fluid which formed an one-dimensional interface; this is fundamentally different from classical pinning and depinning in which a pinnned three-dimensional medium applies force to an interface area that translates to "the square of the length of distortion" [13]. This difference allows the three-dimensional droplet to depin and rapidly move the contact line forward, whereas two-dimensional lipid bilayer was not able to depin but rather cirumflowed the pining

center.

1.4.2 Experiments with Al_2O_3 hydrophobic barriers

In 1999, Nissen et al suggested that "a large number of pinning centers should hinder and eventually stop membrane spreading" [13]. They proposed that "for a given spreading parameter stable arcs of radius θ/S must be form between two pinning centers, whereby θ denotes the one-dimensional line tension." [13] They further studied pinning in an experiment in which they placed hydrophobic aluminum-oxide barriers (7 μm in diameter and 25 μm spatial periodicity) in the path of a spreading lipid front; the number was not great enough and just like previously observed, the bilayer spread through the interstitial space and then grows back to the obstacle [31].

1.4.3 Diffusion across narrowly pinned space

There has been no work in literature studying lipid spreading percolation threshold into nanoparticle arrays. However, if we consider diffusing across pinning centers as a form of "percolation", Lohmüller et al.'s work in 2011 would provide some insight. By vesicle fusion, bilayers were deposited onto surfaces with gold nanoparticle arrays with inter-particle spacings that range from 58 nm to 151 nm. When Texas-Red probe was used, fluorescence recovery after photo-bleaching (FRAP) tests found no difference in diffusion across differing nanoparticles density, but for bilayers doped with His12-mGFP, a small trend for faster diffusion on larger particle spacing was exhibited [32].

Chapter 2

Materials and Methods

2.1 Formation of lipid gradients

In this study, lipid component gradient over a surface of bilayer was created by stamp spreading two stacks of different lipids at close proximity so that the bilayers spread out, collide into each other, self-heal and become one membrane, and starting in the collision point the individual lipid molecules diffuse and mix across the original collision line. Professor Babak Sanii and former lab members Jose Cortez and Katherine Liu has pioneered this method .

2.1.1 Stamp design

A mechanical deposition of lipid stacks was preferred for the purpose of systematically creating bilayer front collisions in timely manner and to ensure that collisions take place at locations close enough to original stack sources so that there are substantial lipid molecules coming from the source to diffuse readily; if reservoir is lacking, lipid front would not spread further while sacrificing the intermolecular interactions within the membrane [8]. To this end, we used rapid-prototyping techniques to create PDMS (poly-dimethylsiloxane) stamps with protruding ridges where lipid mixtures are deposited and

subsequently stamped from. For the two-way, linear collisions in this study, the design of a pair of parallel ridges 0.75 millimeter apart was employed.

2.1.2 Use of laser engraver to create stamp molds

We use a consumer-grade laser-cutter(Full-Spectrum Engineering H-series) to implement our mold designs before filling them in with PDMS. For experiments in this study, each lipid-depositing ridge was implemented on the associated software (Retina Engrave) by placing two line adjacent to each other; this can be easily done by drawing lines and prescribing the location mechanically 0.01 units apart from each other. We engrave two adjacent lines for each ridge because this creates only enough cavity in the mold to produce a stable PDMS ridge that is firm enough for stamping and wide enough for lipid deposition. Quite inconveniently, the design function in this software uses a unit system that is equivalent to 0.538 centimeter per unit, so aside from prescribing lines adjacent to each other, any other prescription of distances has to be converted. Finally, we found raster engraving transparent acrylic at a speed setting of 90 percent and power setting of 60 percent produces the best molds for stamp production.

2.1.3 Manufacturing of stamps

We use the elastomer polydimethylsiloxane (PDMS, Dow Corning Sylgard 184), mixed along with 10 % by mass of curing agent, to produce the stamps. It comes in a liquid-gel form that can be pour into any mold, and it solidifies and maintains the mold shape as it hardens after baking. This mixture was poured uniformly onto the acrylic stamp molds until the mixture overflows off the sides of the mold and was baked for two hours at 80 °C. After baking, the PDMS layer, along with its protruding features, was peeled off the mold, cut, wiped-clean with ethanol, and sticked by double-sided tape onto small binder clips for ease of handling.

2.1.4 Inking the stamp with lipids

We store lipids in ethanol at -20 °C and sonicate them for three minutes before each use. Lipid mixture is calculated by percent molar weight and physically mixed by a combination of pipetting, vortexing, and sonicating until mixture appear homogeneous. Lipids in ethanol were carefully deposited onto stamp ridges by microsyringes, usually 1 microliter per 0.6 mm ridge. Lastly, "inked" stamps were desiccated for two hours to ensure evaporation of ethanol.

2.1.5 Preparation of substrates

Experiments in this study was for the most part conducted on glass cover slips, although there were a few exception of stamping on silicon surfaces. In either case, substrates were activated by plasma immediately before stamping. The 3-minute treatment should give the surface a negatively-charged, hydrophillic character.

2.1.6 The stamp spreading method

Desiccated lipids were stamped manually onto the plasma-treated surfaces, making sure that all the ridges have made contact with the surface. Stamps were pulled upward vertically after contact to avoid smudging. Immediately afterwards, phosphate buffered saline (PBS, 10 mM phosphate buffer, 2.7mM KCl, 137 mM NaCl, pH 7.4, Bioland Scientific LLC) was added to submerge cover slips and lipids. From this point on and for the remainder of the experiment, whether through heating, medium changing, or imaging, we made sure the cover slips were submerged under liquid as exposure to air would peel off the lipid bilayer [9].

2.1.7 Use of fluorescence for observation

One advantage of the SLB model is the ease of imaging through fluorescence microscopy [8]. We used a home-built, low cost fluorescence microscope (SwingScope [33]) to image from the bottom-up. Although top-down imaging was possible, a bottom-up approach through transparent glass eliminates the shakiness of imaging through water. The two fluorescent labels we used for our bilayers were *N*-(7-nitrobenz-2-oxa-1,3-diazol-4-yl)-1,2-dihexadecanoyl-*sn-glycerol*-3-phosphoethanolamine triethylammonium salt (NBD-DHPE, biotium) and *N*-(Texas Red sulfonyl)-1,2-dihexadecanoyl-*sn-glycerol*-phosphoethanolamine triethylammonium salt (Texas Red-DHPE, biotium); NBD-DHPE was usually used at 3% concentration by mass, whereas Texas Red-DHPE was used at 1% or less.

We further capitalize on this character by using fluorescence as a method to track diffusion. For example, as we conduct a collision of two lipid stacks, we would dope one bilayer with fluorescence and and leave the other unlabeled; in this way, as the two bilayers collide and diffuse, we can observe molecules from the fluorescent-labeled stack diffuse into the unlabeled bilayer and use fluorescence intensity profile to track the degree of equilibration. The same method had been used in conjunction with Fick's Second Law of Diffusion, Fourier transform, and error function to determine diffusion coefficient of the bilayer to be 2.4 $\mu m^2/s$, which is in agreement with literature values [18].

2.2 Formation of lipid domains by spreading gradients

2.2.1 Lipid components

For the majority of this study, lipid domains were formed with bilayers composing of POPC, GalCer, cholesterol, and the fluorescent probe Texas Red-DHPE. The domain-forming stack consisted of 64% POPC, 27% GalCer, 8& cholesterol, and 1% Texas Red-

DHPE, and it collided with a bilayer of 100% POPC to form a bilayer in which the intermediate region between the two stacks saw a gradient of decreasing GalCer, cholesterol, and Texas Red DHPE components.

"GalCer (bovine cerebrosides, a mixture of nonhydroxylated and hydroxylated GalCer, 75% saturated and 25% singly unsaturated, with tail lengths varying from 18 to 27 carbons (see 2005/2006 Matreya handbook, p. 92, Cat #1050, for exact percentage of each tail length)) was purchased from Matreya (Pleasant Gap, PA). POPC, DPPC, and cholesterol were purchased from Avanti Lipids (Alabaster, AL) [25].

2.2.2 Temperature bath

Temperature control was achieved by submerging sample, immediately after stamping and hydration, into a 400-mL PBS bath heated to approximately 50°C [25]; the entire system (the lipid bilayer on glass cover slip in 400-mL PBS bath) was then let cool in room temperature. An Arduino temperature logger (built by Professor Babak Sanii) was used to track temperature every 30 seconds. A sample cooling profile is presented in Figure 2.1. Temperature experienced by the sample was assumed to have jumped to 49°C immediately after submergence and was cooled to near-room temperature of 30°C over 3.5 hours, with average cooling rate of 0.08°C/minute and maximum cooling rate of 0.13°C/minute at the start of cooling.

2.3 Deposition of gold nanoparticles on glass

Dr. Theobald Lohmueller has developed a procedure to uniformly deposit gold nanoparticles on glass or silicon substrates [34], and a large part of this procedure was conducted with the assistance of his student Anastasia Babynina.

The general concept of the procedure is to dissolve block copolymers in toluene, which form micelles of nanocompartments capable of loading single metal precursors such as

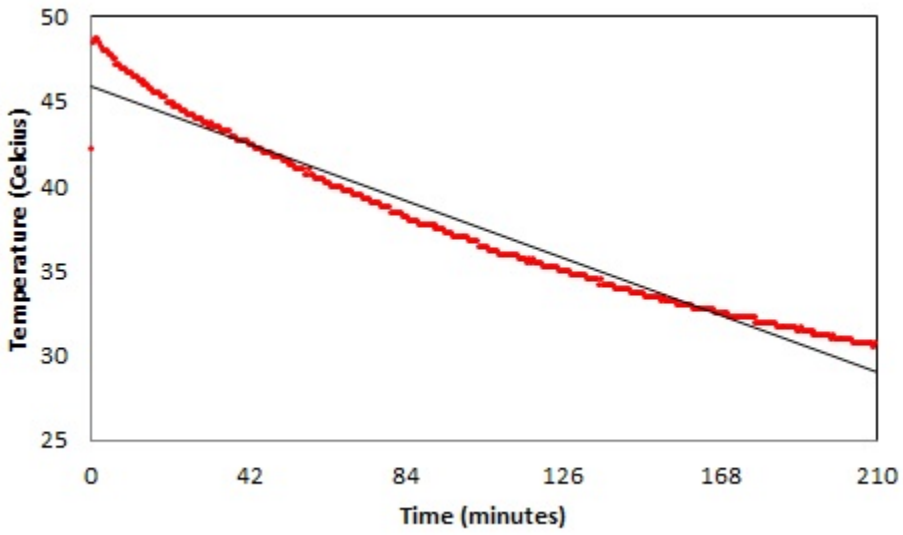

Figure 2.1: Temperature profile of sample slow-cooling. Red data points indicate temperature of bath every 30 seconds. Linear best fit demonstrate an average cooling rate of 0.08°C/minute with an R^2 value of 0.9665, whereas a quadratic fit results in the equation of $y = 0.0003x^2 - 0.1343x + 47.974$ with an R^2 value of 0.9957.

single gold nanoparticles [35]. Addition of this micellar solution to substrates creates a self-assembled monolayer of hexagonally-packed micelles upon solvent evaporation [36]. Lastly, copolymers were removed by plasma treatment, and the uniform array of nanoparticles remain.

2.3.1 Preparation of polymer solution

Block copolymer polystyrene(1056)-block-poly(2-vinylpyridine)(486) from Polymer Source Inc., Montreal, Canada was dissolved into 20 mL of toluene at a concentration of 3 mg/mL. Dissolution was achieved by stirring 24 hours in a PTFE-sealed beaker, after which block copolymers should exist as micelles each with a compartment capable of loading metal precursors.

2.3.2 Addition of gold nanoparticles

Gold-(III)-chloride hydrate (Sigma Aldrich, Taufkirchen, Germany) was added to the toluene-block copolymer solution. Solution was stirred 72 hours in a PTFE-sealed beaker.

2.3.3 Preparation of substrates

Glass and silicon substrates were rigorously cleaned in a process that included a 30-minute sonication in 2% Helmanex at 45°C, a 15-minute sonication in MilliQ water at 45°C, and subsequent blow drying and plasma cleaning.

2.3.4 Dip-coating

After the gold nanoparticles-loaded micelle solution was prepared, micelles can be deposited onto the plasma-cleaned substrates in two ways. One of these ways was dip-coating, which involves an electric apparatus that slowly dips a substrate into and subsequently out of the solution. Toluene evaporation as substrate was slowly pulled out of the solution should leave a monolayer of hexagonally-arrayed micelles on both sides of the substrate. A feature of this method was that only a little bit more than half of the surfaces of the substrates would be deposited with the micelles because we didn't want to go to far and also dip the apparatus clip into the solution. We ended up using this feature to our advantage by stamping a ridge of POPC stack on the dipping edge to study the effect of deposited gold nanoparticles on lipid spreading.

2.3.5 Spin-coating

The other deposition method was spin-coating, which employs a spin-coater for centrifugal force to evenly disburse the small amount of deposited material from the center onto the entirety of the surface. This method deposited material on only one side of substrate, but the entirety of the treated side was deposited evenly with gold nanoparticles.

Both dip-coating and spin-coating were conducted in this study, but Dr. Lohmueller and Anastasia determined that dip-coating created better results so further experiments exclusively used dip-coated samples.

2.3.6 Plasma treatment to remove polymer

Using a Femto low-pressure plasma cleaner from Diener Electronic, samples were treated for 45 minutes in air-plasma. This step was supposed to deposit the gold nanoparticles by removing the polymer shell around them. To ensure removal of all polymer, a full 45-minute treatment of plasma with the right plasma cleaner was required, if not more. Samples in this study was plasma cleaned for 45 minutes, yet their purity was questioned because the pink color still very much represented polymer residue on the surface.

2.3.7 Imaging with nano-scale microscopes

Scanned electron microscopy (SEM) measurements were conducted on three dip-coated samples and two spin-coated samples. Since the operation of a SEM was difficult, Anastasia Babynina assisted me greatly in achieving these measurements. Four months after samples were produced, an attempt was made to confirm SEM findings about gold nanoparticles by imaging with ezAFM (easy to use atomic force microscope, NanoMagnetic Instruments). Preliminary measurements were able to focus on the samples, but no gold nanoparticles were detected due to lack of experience with the microscope and lack of time to master it.

Chapter 3

Results

3.1 Lipid domain gradients

3.1.1 Gradient of domains

In a simple two-way bilayer collision experiment (Figure 3.1), we created a healed bilayer with compositional gradient that ranges from 64% POPC, 27% GalCer, 8% cholesterol, and 1% Texas-Red on the right to 100% POPC on the left. The entire collision experiment was conducted in conjunction with a temperature control similar to that profiled in Figure 2.1; as soon as lipid was stamped and hydrated, the entire petri dish was submerged into a 400-mL PBS bath that had already been heated to 51 °C and then left in room temperature to cool. After the slow-cooling process, collision area was recorded by fluorescence microscopy with the Texas-Red settings (Figure 3.1a).

Figure 3.1a exhibited a Texas-Red fluorescence intensity gradient as the background went from dark to bright from left to right. In an Octave program written by Dr. Babak Sanii (see Appendix A), local lipid composition was estimated by relative fluorescence intensity at the location. Individual domain shapes were identified by the same Octave program, and domain areas and area/perimeter ratios for each domain were plotted over GalCer and cholesterol component percentage.

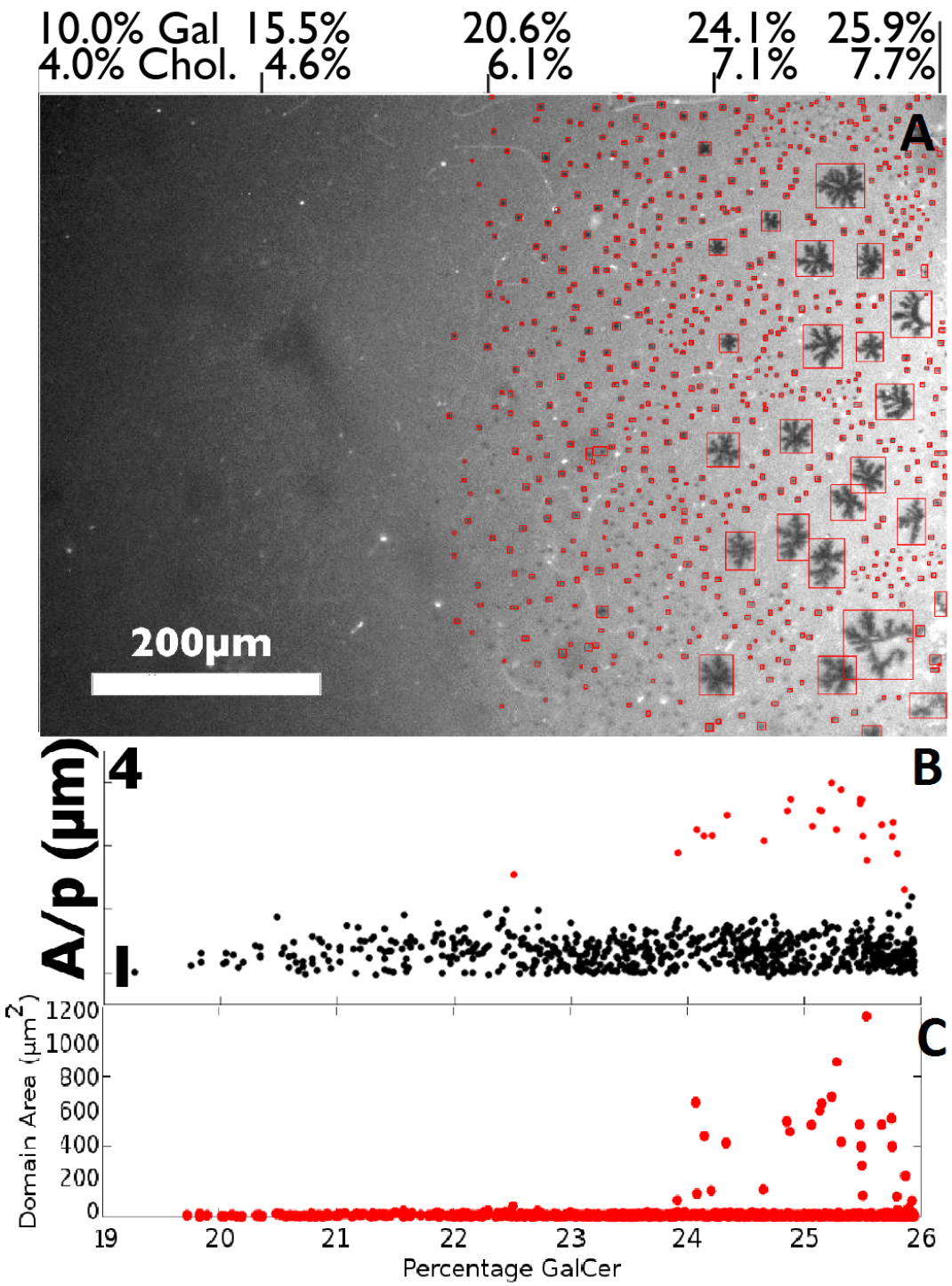

Figure 3.1: Collision of (left) 97% POPC, 3% NBD-PE and (right) 63.8% POPC, 27% GalCer, 8% cholesterol, 1.2% Texas-Red. (a) Fluorescence image of collision zone. (b) Area/perimeter ratios of domains across composition gradient. (c) Individual domain areas across composition gradient.

As predicted from the decreasing GalCer component, the gradient observed a decreasing area coverage by GalCer domains from right to left; in fact, with our fluorescence microscopy and labeling approach, no GalCer domains were visible at GalCer compositions less than 19%. Similar to Szmodis et al (2010), we observed two modes of domains in terms of shape and size [26]. A category of larger, more dendritic domain has individual areas that range from 200-1200 μm^2, which contrasts a category of smaller domains that are mostly less than 100 μm^2 in size (Figure 3.1c). The fractal-like features of the larger domains extend the perimeters of these domains, but they do not seem to produce a substantial decline in the area/perimeter ratios from the denominator. As such, the category of larger domains, plotted as red dots in Figure 3.1, have higher area/perimeter ratios than the category of smaller domains, plotted as black dots. Dendritic features were not observed in the smaller domains, possibly a natural attribute of small domain formation or lack of microscopy capabilities to visualize nano-scale features.

3.1.2 Gradients of domain-forming components

To further apply and test out the robustness of the gradient platform, we engineered three more collisions that varied the cholesterol (Figure 3.2a), GalCer (Figure 3.3a), and Texas-Red (Figure 3.3b) concentrations across the collision-diffusion zone. We compared our observation of domain phase behaviors with those published in literature and found similar results.

We were especially interested in comparing cholesterol gradient against the interesting dip in domain sizes around 3 to 5 % cholesterol content. In Figure 3.2, we collided two POPC bilayers with the same 27% GalCer content but one also contain 8% cholesterol content while the other did not. Due to my inability to construct another Octave program to analyze this image as in Figure 3.1, the result is analyzed by ImageJ fluorescent plot profiling for estimation of cholesterol component (Figure 3.2b), ImageJ Auto Local Threshold for distinction of darker domain regions (figure part c), ImageJ Analyze Par-

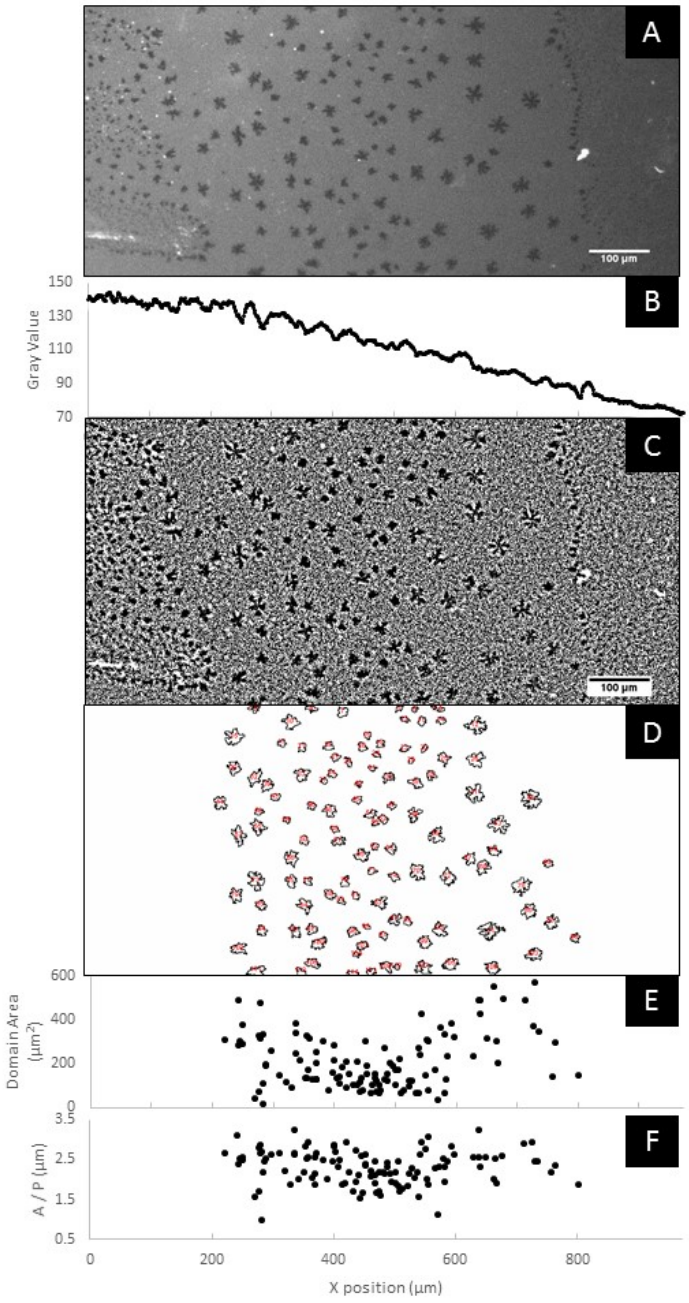

Figure 3.2: Collision of (left) 64% POPC, 27% GalCer, 8% cholesterol, 1% Texas-Red and (right) 73% POPC, 27% GalCer. (a) Fluorescence image of collision-equilibration zone. (b) Fluorescence intensity profile over space. (c) ImageJ "Auto Local Threshold" result (Median method with radius 7). (d) ImageJ "Analyze Particles" (Size 10 to infinity pixel^2), resulting particles outline. (e) Individual domain areas over space. (f) Individual domain area/perimeter ratios over space.

ticles for identification of individual domain shapes (Figure 3.2d). Using the measured domain areas and perimeters from the domain shape outlines (Figure 3.2d), domain areas and area-over-perimeter ratio were plotted against position X. Because we used a slower cooling rate for domain formation, our domains were much bigger than those observed by Lin et al [25, 26]. This resulted in values a few times bigger than Lin et al's published data, but we saw a similar trend in which domains in the middle of the 0 to 8% cholesterol

gradient exist in smaller shapes and become bigger on either ends. On the other hand, the smaller domains do not have dendritic structures like the big domains do, possibly due to (1) lack of fluorescent microscope capabilities to see nano-scale structures or (2) limiting forces of inter-facial line tension.

Gradients of GalCer and Texas-Red were ran more as a control (Figure 3.3) to validate the robustness of our gradient approach. As such, only qualitative analyses were conducted. Because GalCer is the main component that makes up a lipid domain, we expected individual domain size to vary along with composition [26]. In Figure 3.3a, from left to right we see a gradient of domain loss, but we did not see as big a change in domain shapes and sizes as we would have expect from a gradient of 27 to 0% GalCer. Closer inspection points out that even on the left side of the image adjacent to the stamp, domain area coverage overall was lesser than we would have expect from a composition just less than 27% GalCer. This may be due to a slower spreading speed for a bilayer with high gel-phase GalCer content compared to a bilayer with just liquid POPC; since spreading and collision were not tracked live, I would not have known if collision took place left of the middle point between the stamps as I had wished them to. Even after the collision, POPC may have a higher activity to diffuse into the new membrane than GalCer which moves slower. Hence there was no large, dendritic domains adjacent to the left stamp as one would have expected for a stack that consists of 27% GalCer.

On the other hand, Figure 3.3b produced more of the results expected. Only 1% fluorescence probe was varied across the collision experiment, and likewise it appears fluorescence was the only feature that changed from left to right. Across the collision zone, there is an equal distribution of large, dendritic domains and small, compact domains.

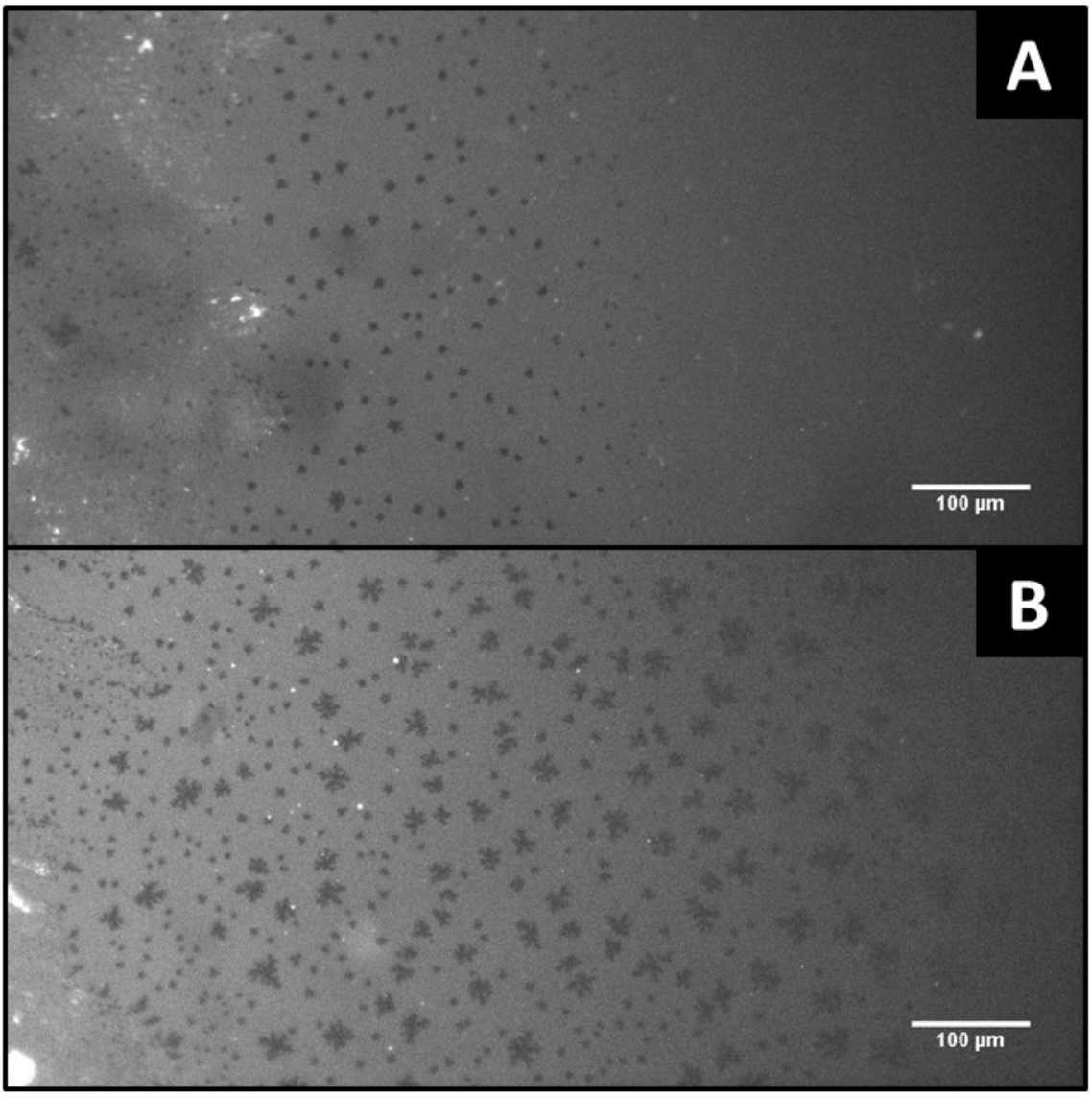

Figure 3.3: (a) Compositional gradient of GalCer: left stamp consisted of 64% POPC, 27% GalCer, 8% cholesterol, 1% Texas-Red and right stamp was 92% POPC, 8% cholesterol. Gradient of Texas-Red probe was to facilitate local composition estimate. (b) Compositional gradient of Texas-Red: Left stamp consisted of 64% POPC, 27% GalCer, 8% cholesterol, 1% Texas-Red and right stamp 65% POPC, 27% GalCer, 8% cholesterol.

3.2 Percolation threshold

3.2.1 Deposition of gold nanoparticles

We dip-coated and spin-coated substrates with a toluene solution of block copolymer gold nanoparticles, and after a final plasma treatment step, the surfaces were ready to

use. We randomly chose a few samples from the batch for quality-assurance survey with scanned electron microscopy (SEM), atomic force microscopy (AFM), and water droplet test.

SEM was conducted on both dip-coated and spin-coated substrates (Figure 3.4, top row). Each gold particle was 10 to 20 nm in diameter. Inter-particle distance for a given nanoparticle was measured by its distance from the nanoparticle closest to it; with 50 random nanoparticles each, we found that on the dip-coated sample, the average interparticle distance was 38 $\pm$ 8 nm, while the spin-coated sample has an average interparticle distance of 35 $\pm$ 8 nm; an equal variance t-test revealed a significant difference between the means (Figure 3.4, bottom row). Qualitatively, we observed nanoparticles were deposited in roughly hexagonal array for both methods, but the dip-coated substrate looked slightly more uniform than that spin-coated. For this reason, unless otherwise noted, we chose to conduct all lipid spreading experiments on the dip-coated substrates; one exception for use of spin-coated sample would be the the AFM measurement conducted four months later since all other dip-coated substrates were consumed by that point.

For further testing of gold nanoparticles stability [37], AFM was conducted approximately four months after the original deposition (Figure 3.5). Evidence of nanoparticles was observed by circular protrusion from the surface as well as by evidence of AFM tip applying too much pressure and pushing materials around [38].

To confirm polymer removal in the final 30-minute plasma treatment step , we deposited a 30-μL milliQ water droplet onto our substrates. On glass where no gold nanoparticles had been deposited, we observed a contact angle of 54°, and on the bottom portion where gold nanoparticles were deposited, the contact angle was 67°. This indicates that both areas are hydrophilic since water droplet contact angle was less than 90°, but the area deposited with gold nanoparticles may be less so. Qualitatively, faint pink-color was observable in area below dipping edge, which may suggest incomplete removal of polymer. Immediately before each lipid stamping, we plasma treated substrates in

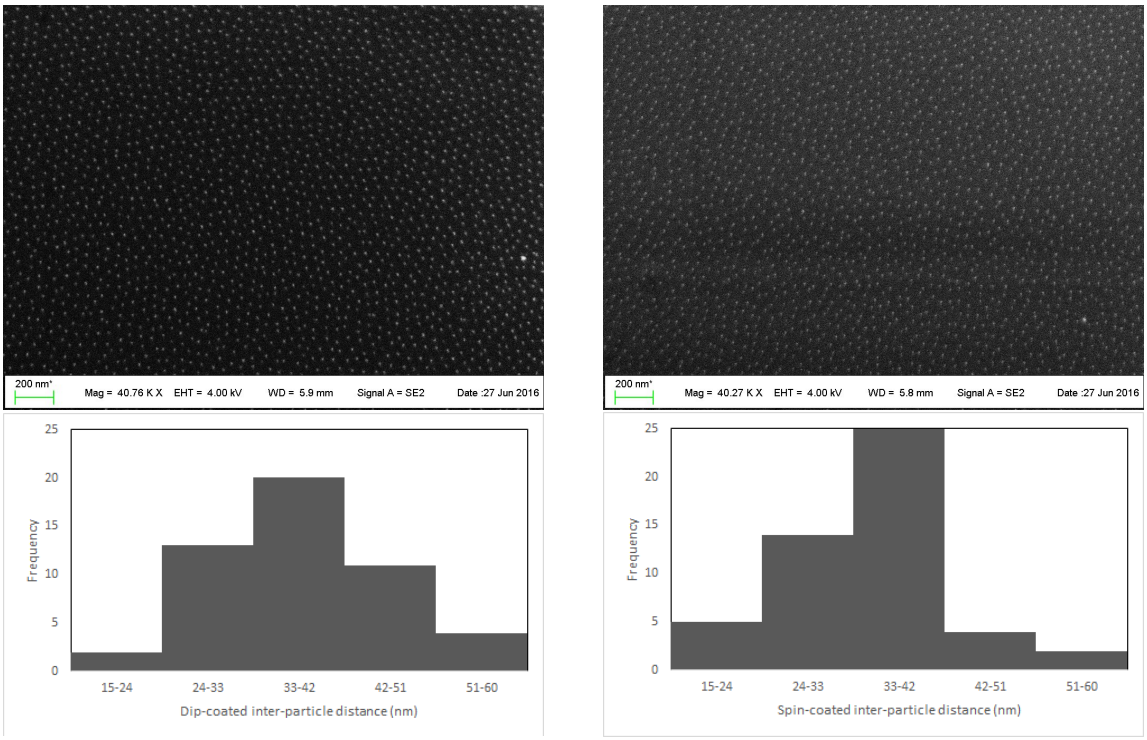

Figure 3.4: Top row: Scanned electron microscopy images of gold nanoparticles deposited on glass through dip-coating (left) and spin-coating (right). Credit to Anastasia Babynina for taking these images on glass without coating on electrically conducting material, which was a very labor-intensive and time-consuming process. Bottom row: Inter-particle distance of 50 random nanoparticles samples.

oxygen for three minutes to activate surface for spreading, so we also conducted a water droplet test immediately after plasma-activation; we found that in this case water droplet flattens out upon contact of substrate, and it did so a bit more on glass that with bare surface than those deposited with gold nanoparticles. Overall, we found that polymer may not have been completely removed by the 30-minute plasma treatment process, but the nanoparticles-deposited surface should still be solid enough for lipid to spread on as bilayer or monolayer [39].

3.2.2 Difference in spreading

We stamped a ridge of POPC, doped with 1% Texas-Red, on a glass slide dip-coated with gold nanoparticles (Figure 3.7). At the dipping edge, we used fluorescence microscopy

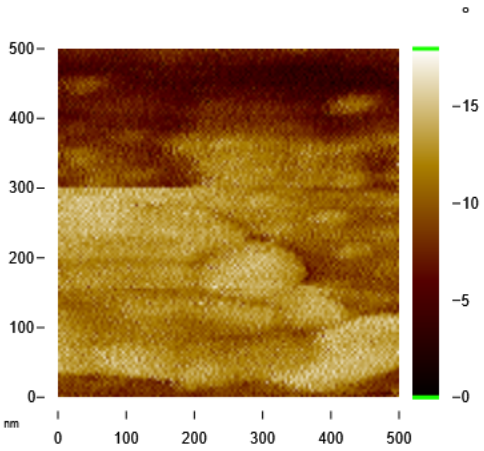

(a) In a close-up view, evidence of gold nanoparticles was observed by circular protrusions from the surface along the right and top edge of the image.

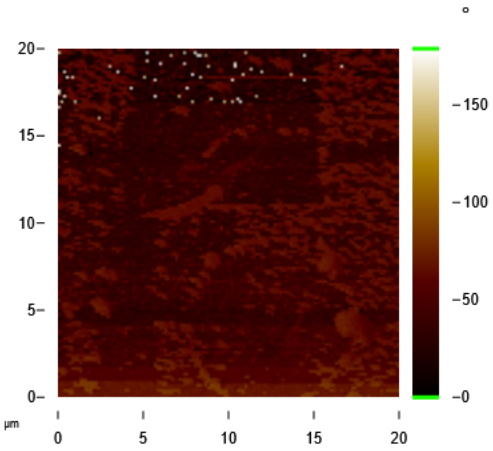

(b) After applying pressure and pushing with the AFM tip in rectangular regions, a zoom-out view revealed the rectangular region where pressure had been applied.

Figure 3.5: Atomic force microscopy of substrate showed evidence of gold nanoparticles four months after deposition.

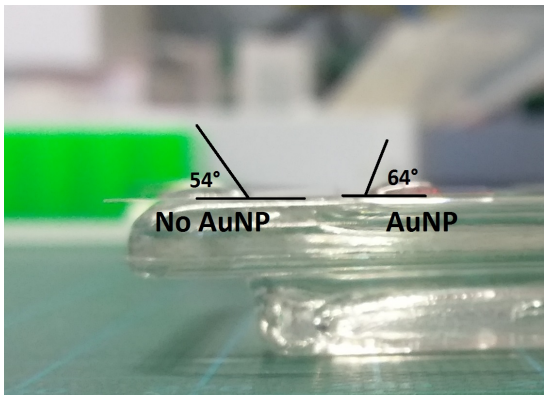

(a) Left droplet was deposited on glass without gold nanoparticles, right droplet was on glass with gold nanoparticles.

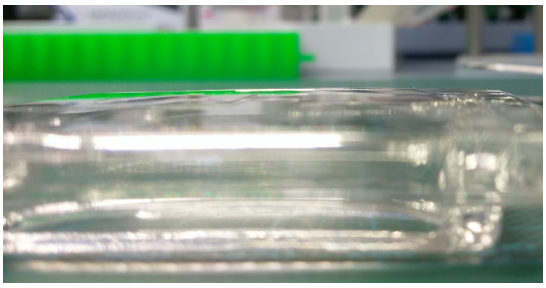

(b) Immediately after plasma activation, water droplet flattens out on both surfaces.

Figure 3.6: Water droplet test of substrates to test hydrophilicity and complete removal of polymer.

to observe bilayer spreading. We found that on the side we dipped where average interparticle distance was narrower than 40 nm (Figure 3.4), the bilayer was not able to spread at all. In fact, a well-defined dipping edge was observed where on the glass side lipid was spreading in every direction away from the stack source, but the only region it could not spread into was the half of the substrate that has been deposited with nanoparticles.

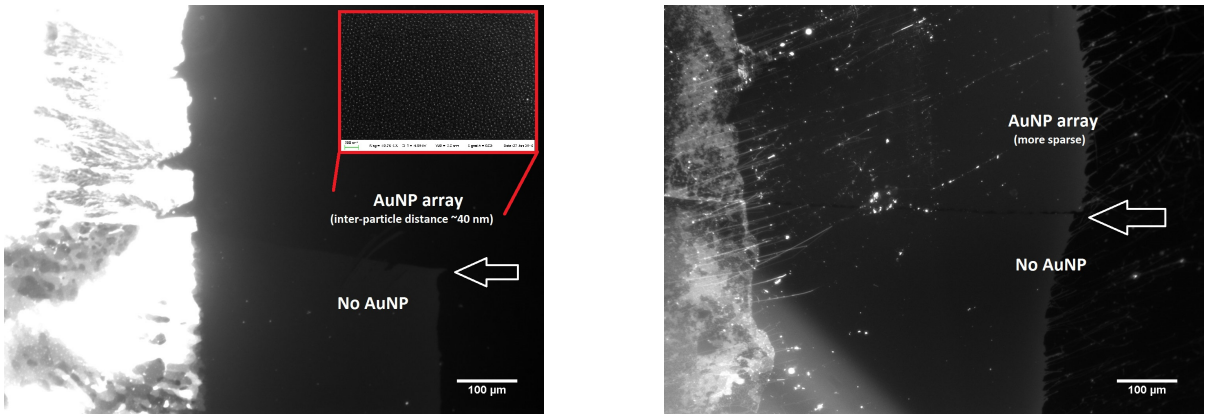

Figure 3.7: POPC bilayer spreading at nanoparticles dipping edge (indicated by white arrow). On the left image where gold nanoparticles were densely deposited, we observed a lipid front spreading only on the bottom non-particle side. On the right image where gold nanoparticles array was supposedly less dense, we observed equal spreading on both sides of the dipping edge.

This surprising finding of POPC not spreading was repeated on spin-coated glass and silicon we prepared in the same batch, and both found POPC not spreading.

On the substrate samples provided by Dr. Lohmüller, of which the supposed average inter-particle distance was 100 nm, we observed equal spreading on both sides of the dipping edge. Interestingly, the dipping edge was well-defined as a dark line dividing the bilayers, which gives us at least some confidence of the nanoparticles existence [32].

3.2.3 Difference in diffusion

Fluorescence recovery after photo-bleaching (FRAP) was conducted twice for POPC bilayers (labeled with 1% Texas-Red) on each of the four surfaces: both nanoparticle side and glass side of the dip-coated substrates prepared for this project, as well as both nanoparticle side and glass side of the substrate sample provided by Dr. Lohmüller. Of the limited data, we found that on the substrates prepared for this project, the mean diffusion coefficient D for the nanoparticles side was 0.33 $\mu m^2/sec$ and for the glass side was 1.35 $\mu m^2/sec$, which are significantly different according to t-test; on the substrates provided by Dr. Lohmüller, diffusion coefficients for nanoparticles side was 1.12 $\mu m^2/sec$

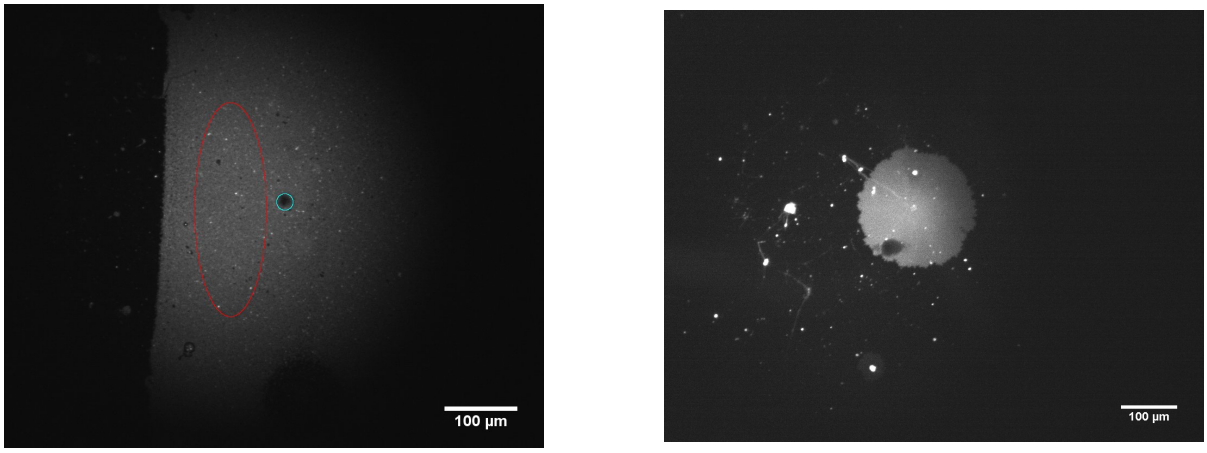

Figure 3.8: Fluorescence recovery after photo-bleaching (FRAP) of bilayers with embedded nanoparticles. Left image depicts a typical FRAP, in which the fluorescence of a photo-bleached area (blue circle) was tracked over time alongside another area of regular diffusion (red oval). Right image is an island of lipid that had incidentally landed onto the dense particle surface that bilayers do not spread into; fluorescence recovery of dark circle on the lower left of the island was especially slow.

and for glass side was 1.16 $\mu m^2/sec$, which are statistically equal according to t-test. For the substrates provided by Dr. Lohmüller, the values differ slightly from previous finding by Lohmüller et al (2011) that diffusion coefficients were 2 $\mu m^2/sec$ for Texas-Red probe regardless of particles densities, but our results do agree, that in principle diffusion was the same for nanoparticles and glass sides. However, for the substrates prepared for this study in which inter-particle distance is less than 40 nm, diffusion was considerably slower.

Chapter 4

Discussion

4.1 Application of lipid gradients

Results from the collision experiments suggest that the gradient platform was effective in using one single experiment to probe general phase behavior over a certain range of concentration. The Texas-Red varying experiment, Figure 3.3b, was the most controlled experiment in which spreading speed of the bilayers should be equal, and likewise results were straightforward as expected. For the cholesterol varying experiment, the gradient platform demonstrated its usefulness by identifying the general trend of domain phase behaviors from 0 to 8 % cholesterol; in contrast, Lin et al. (2007) had to run at least four experiments to arrive at the same trend. However, the ability of programming to estimate local cholesterol concentration in accordance with fluorescence intensity would have added more validity to the data. The experiment varying 27% Galcer to 0% illuminates a limitation of the platform: if the two colliding bilayers have differing spreading speed, they would collide not in the midline but somewhere towards the slower-moving bilayer. Since by experience it was known that GalCer partitioned bilayer spread slower, one way this experiment could have been improved was to lesser the variation in stamp GalCer compositions (for example, a collision of 27% to 15% Galcer) so that spreading could

be more equlibrated. Another possible solution would be to lengthen the collision zone so that the POPC-rich bilayer would have to travel further, diminish more of its stack source before reaching its counterpart bilayer.

4.2 Lipid domains formation

We observed the same trend as Lin et al. (2007) of decreasing and then increasing domain sizes as cholesterol varies from 0 to 8% [25]. This provides us a better understanding of how cholesterol partition within our model membrane of GalCer domains in POPC surroundings and how different partitioning affects the impact of line tension.

In slow-cooling our domain-forming bilayers, we observed the effect of significant domain growth such that there existed two modes of domains: a larger, dendritic type and a smaller, circular type [26]. Unfortunately, the process of slow-cooling happened in a covered beaker, or it would have been interesting to see domains grow in vitro like Szmodis et al. (2010). This might be achievable in the future with the successful implementation of the nanoparticle localized heating function; perhaps we could gain some insight on the mechanisms of domain growth, whether it be by coalescence of smaller domains or by Ostwald ripening [40]. After all, in all our experiments, there does exist a significant area of domain-free zone immediately surrounding each large, dendritic domains. In addition, it was interesting to confirm that in the short-term, GalCer-GalCer interaction was stronger than the limiting forces of line tension that would have keep it from growing [26]. It would be worthwhile to track these domains over an extended amount of time to see how line tension slowly relaxes their rosette shapes to become more circular [41].

4.3 Percolation threshold for lipids

When attempting to spread POPC bilayer on the gold nanoparticles surface Anastasia and I prepared, we encountered the surprising result that POPC would not spread on

surfaces with average gold particle spacings below 40 nm. Literature has found normal diffusion in spacing as narrow as 58 nm, but spacing below 40 nm has not been experimented with in literature. If we can confirm that the polymer residue does not interfere strongly with lipid spreading, we might be able to prove that the 40 nm spacing was below the percolation threshold. Another limitation to our finding was that the substrate samples provided by Dr. Lohmüller were a few years old, and there was not enough time nor sample to conduct another SEM to confirm spacing of gold nanoparticles. However, if all our assumptions were true and the percolation threshold was just above 40 nm, the fact that lipid does not spread into them below the threshold may suggest that lipid bilayers form pores surrounding nanoparticles and do not go over above them in spreading [42]. In any case, it would be worthwhile to validate all the uncertain elements of this experiment to see if there really is a percolation threshold for lipid bilayers.

Chapter 5

Future directions

5.1 Experiment to study cholesterol partitioning in domains

In this thesis I varied cholesterol concentration from 0 to 8% and found the interesting dip in gel-state domain size. Pass 8%, Lin et al. observed liquid-liquid state domains starting at 10%, and their Figure 3b (see Figure 1.1) predicts bilayer to be in uniform liquid-disordered phase pass 18% cholesterol. If gradient platform allows for collision of 0% to 20%, or at least 12% cholesterol to work, it would be interesting to observe gel-phase and liquid-phase domain in the same image.

5.2 Engineering a three-way collision for triangular phase diagram

In this study we created gradients that manipulated the lipid components individually. As we master this technique, the next step would be to engineer a three-way collision experiment to solve for a ternary phase diagram in one single experiment. One would have to consider the spreading speed of components as well as fluorescent probing method

for the additional bilayer, and maybe use the available rapid prototyping techniques for fine-tuning.

5.3 Application of lipid bilayers and plasmonic nanoparticles in cell studies

A direction that has not changed since this project is to create a dynamic surface of nanopatterns that may be useful in cell studies. The first step would be to successfully lay down a lipid bilayer on a surface deposited with gold nanoparticles (or any metal nanoparticles or nanorods), which this thesis has shown signs of doing with the glass coverslips provided by Dr. Lohmüller. Following would be to test out the plasmonics heating property on lipids and find the best to implement them in practice. After mastering these skills, it would be relevant to collaborate with micro-patterning to design a surface that is worth studying.

Chapter 6

Conclusion

In this thesis, the collision-gradient method was used to probe lipid bilayer physical behavior by varying each lipid component. We found that the key to ensure the success of the collision-gradient method was to not vary the lipid components too much as to end up with disparate speed of spreading before collision; if large concentration variation was desired, one could engineer details so that collision and diffusion happen at the desired data-collecting location. In spreading lipids on gold nanoparticles array of 40 nm inter-particle distance, a percolation threshold could have potentially be found despite several uncertainties.

6.1 Acknowledgments

First, I thank God Above for Your love and mercy, for allowing me to study the creation you have made.

I would like to thank Dr. Babak Sanii for giving me the opportunity to do research since my first college summer and continue working with me, guiding me, teaching me all the way till senior year. Thank you for sharing with me your passion for your career and your attitude towards life. I cannot thank you enough for the opportunities these years of mentorship has led me to and will continue to inspire me towards in the future.

Thank you also to Prof. Dr. Joachim Rädler, for inviting me to do research at Munich this summer and offering to be my primary thesis reader.

I would also like to thank all the people I worked with at the Self-Assembly lab at Keck Science Center in Claremont, California and at the Faculty of Physics at Ludwig-Maximilians University in Munich, Germany. Special thanks to Katie Liu and Michael Swift for introducing me to the world of lipid spreading, to John Rizzo and Victoria Nguyen for your support on the SwingScope, to Alex Fink for supervising me around at LMU, to Dr. Theobald Lohmüller, Anastasia Babynina, and Patrick Urban for your guidance and help on plasmonics gold nanoparticles, to Phiip Böhm, Chrissy Dirscherl, and Frank Dauenhauer for your help on lipids, especially with FRAP, and to Charlott Leu for your help in the clean room. This thesis would not have been written today without you all.

Thanks to family and friends for all your support, prayers, and jokes along the way. I love you all very much.

Lastly, I would like to thank all the agencies, including HHMI, CMC's ISS scholarship, and SFB 1032, that has funded me through three summers of research. I really appreciate the opportunity to study a field so extensively as an undergraduate.

Bibliography

(1) Nelson, D. L.; Cox, M. M. In *Lehninger Principles of Biochemistry*, 5th ed.; W. H. Freeman and Company: New York, 2008; Chapter 11, pp 389–390.

(2) Iwasa, J.; Szostak, J.; Bell, T. Exploring Life's Origins: Fatty Acids., 2008.

(3) Nelson, D. L.; Cox, M. M. In *Lehninger Principles of Biochemistry*, 5th ed.; W. H. Freeman and Company: New York, 2008; Chapter 2, pp 48–49.

(4) Nelson, D. L.; Cox, M. M. In *Lehninger Principles of Biochemistry*, 5th ed.; W. H. Freeman and Company: New York, 2008; Chapter 11, p 374.

(5) Nicolson, G. L. *BBA - Biomembranes* **2014**, *1838*, 1451–1466.

(6) Singer, S. J.; Nicolson, G. L. *Science* **1972**, *175*, 720–731.

(7) Brian, A. A.; Mcconnell, H. M. *Immunology* **1984**, *81*, 6159–6163.

(8) Steven G. Boxer *Current Oppinion in Chemical Biology* **2000**, *4*, 704–709.

(9) Cremer, P. S.; Boxer, S. G. *J. Phys. Chem. B* **1999**, *103*, 2554–2559.

(10) Nelson, D. L.; Cox, M. M. In *Lehninger Principles of Biochemistry*, 5th ed., New York, 2008; Chapter 11, pp 381–389.

(11) Richter, R. P.; Bérat, R.; Brisson, A. R. *Langmuir* **2006**, *22*, 3497–3505.

(12) Sackmann, E. *Science* **1996**, *271*, 43.

(13) Nissen, J.; Gritsch, S.; Wiegand, G.; Rädler, J. O. *Eur. Phys. J. B* **1999**, *10*, 335–344.

(14) Kalb, E.; Frey, S.; Tamm, L. K. *BBA - Biomembranes* **1992**, *1103*, 307–316.

(15) Nollert, P.; Kiefer, H.; Jahnig, F. *Biophys. J.* **1995**, *69*, 1447–1455.

(16) Radler, J.; Strey, H.; Sackmann, E. *Langmuir* **1995**, *11*, 4539–4548.

(17) Sanii, B.; Nguyen, K.; Rädler, J. O.; Parikh, A. N. *ChemPhysChem* **2009**, DOI: 10.1002/cphc.200900372.

(18) Liu, K.; Hung, C.-M.; Swift, M.; Mu?oz, K.; Cortez, J.; Sanii, B. *Soft Matter* **2015**, *11*, DOI: 10.1039/c5sm02013a.

(19) Shaw, J. E.; Epand, R. F.; Epand, R. M.; Li, Z.; Bittman, R.; Yip, C. M. *Biophys. J.* **2006**, *90*, 2170–2178.

(20) Nelson, D. L.; Cox Michael, M. In *Lehninger Principles of Biochemistry*, 5th ed., New York, 2008; Chapter 10, pp 343–349.

(21) Fantini, J.; Cook, D. G.; Nathonson, N.; Spitalnik, S. L.; Gonzalez-scarano, F. *Proc. Natl. Acad. Sci. USA* **1993**, *90*, 2700–2704.

(22) Bhat, S.; Spitalnikt, S. L.; Gonzalez-Scarano, F.; Silberberg, D. H. *Proceedings of the National Academy of Sciences of the United States of America* **1991**, *88*, 7131–7134.

(23) Brown, D. A.; Rose, J. K. *Cell* **1992**, DOI: 10.1016/0092-8674(92)90189-J.

(24) Thompson, T.; Tillack, T. W. *Ann. Rev. Biophys. Biophys. Chem.* **1985**, *14*, 361–386.

(25) Lin, W.-C.; Blanchette, C. D.; Longo, M. L. *Biophysical Journal* **2007**, *92*, 2831–2841.

(26) Szmodis, A. W.; Blanchetter, C. D.; Longo, M. L.; Orme, C. A.; Parikh, A. N. *Biointerphases* **2010**, *5*, 120–130.

(27) Richardson, H. H.; Carlson, M. T.; Tandler, P. J.; Hernandez, P.; Govorov, A. O. *Nano Lett.* **2009**, *9*, 1139–1146.

(28) Baffou, G.; Quidant, R.; García De Abajo, F. J. *ACS Nano* **2010**, *4*, 709–716.

(29) Bendix, P. M.; Reihani, S. N. S.; Oddershede, L. B. *ACS Nano* **2010**, *4*, 2256–2262.

(30) Urban, P.; Kirchner, S. R.; Mühlbauer, C.; Lohmüller, T.; Feldmann, J. *Sci Rep.* **2016**, *6*, DOI: 10.1038/srep22686.

(31) Nissen, J.; Jacobs, K.; Rädler, J. O. *Phys. Rev. Lett.* **2001**, *86*, 1904–1907.

(32) Lohmueller, T.; Aydin, D.; Schwieder, M.; Morhard, C.; Louban, I.; Pacholski, C.; Spatz, J. P. *Biointerphases* **2011**, *6*, MR1–MR12.

(33) Nguyen, V.; Rizzo, J.; Sanii, B. *PLoS ONE* **2016**, *11*, DOI: 10.1371/journal.pone.0166735.

(34) Lohmueller, T.; Osinkina, L. Synthesis of quasi-hexagonal arrays of small AuNPs on glass or silicon substrates.

(35) Spatz, J. P.; Mössmer, S.; Hartmann, C.; Möller, M.; Herzog, T.; Krieger, M.; Boyen, H. G.; Ziemann, P.; Kabius, B. *Langmuir* **2000**, *16*, 407–415.

(36) Lohmueller, T.; Bock, E.; Spatz, J. P. *Adv. Mater.* **2008**, *20*, 2297–2302.

(37) Ma, Z.; Dai, S. In *Heterogeneous Gold Catalysts and Catalysis*; Royal Society of Chemistry: 2014; Chapter 1, pp 1–26.

(38) Tafazzoli, A.; Sitti, M. In *ASME International Mechanical Engineering Congress*, Anaheim, 2004.

(39) Sanii, B.; Parikh, A. N. *Soft Matter* **2007**, *3*, 974–977.

(40) Stanich, C. A.; Honerkamp-Smith, A. R.; Putzel, G. G.; Warth, C. S.; Lamprecht, A. K.; Mandal, P.; Mann, E.; Hua, T. A. D.; Keller, S. L. *Biophys. J.* **2013**, *105*, 444–454.

(41) Jeppesen, J. C.; Solovyeva, V.; Brewer, J. R.; Johannes, L.; Hansen, P. L.; Simonsen, A. C. *Langmuir* **2015**, *31*, 12699–12707.

(42) Roiter, Y.; Ornatska, M.; Rammohan, A. R.; Balakrishnan, J.; Heine, D. R.; Minko, S. *Nano Letters* **2008**, *8*, 941–944.

Appendix A

Octave code to analyze Figure 3.1

Octave script to analyze Figure 3.1 was co-developed by Prof. Babak Sanii and student Chen-min Hung, with Prof. Sanii providing most of the coding knowledge.

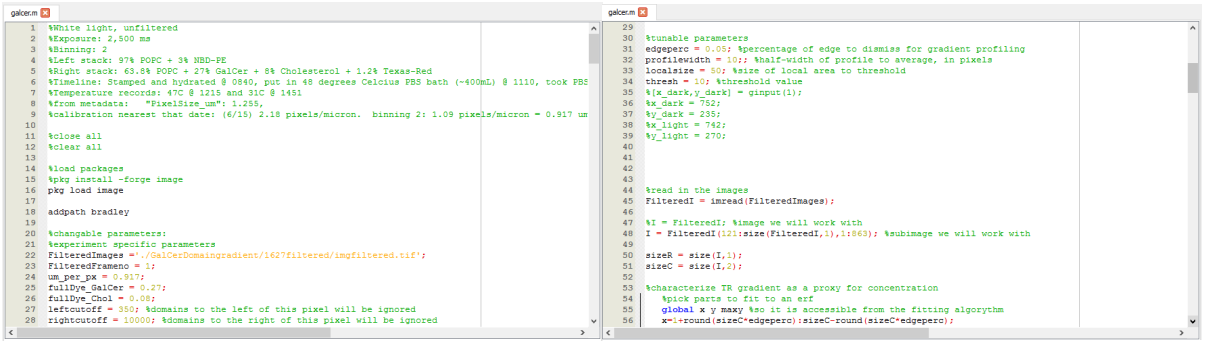

```
%make a threshold image
I_thresh = 1-bradley(I, [localsize localsize], thresh, 'replicate');
I_thresh = bwareaopen(I_thresh,4); %remove things smaller than 4 pixels big
I_thresh(:,1:leftcutoff) = 0;
I_thresh(:,rightcutoff:sizeR)=0;

%ID all things
[L,num] = bwlabel(I_thresh);
props = regionprops(I_thresh, 'Area', 'Centroid', 'FilledArea', 'Perimeter', 'bounding_box', 'Ima

%plot IDs
%  figure
%  imagesc(I_thresh);
%  hold on
%  for i = 1:num,
%  loc = props(i).Centroid;
%  locsize(i) = num2str(props(i).Area,3);
%  text(loc(1), loc(2), locsize);
%  end

%Interpret quantifications
for i = 1:num,
   locarea(i) = props(i).Area;
   locperim(i) = props(i).Perimeter;
   loc(i,:) = props(i).Centroid;
   locgalcer(i) = GalCer_pixels(round(loc(i,1)));
   locchol(i) = Chol_pixels(round(loc(i,1)));
end
```

```
%area/perimeter^2*4pi for each domain
locShape = locarea./(locperim.^2)*4*pi;
usable = locShape<1;%small features that violate the rule
locShapeGood = locShape(usable); %small features that violate the rule
locShapeCorrected = locShape;
locShapeCorrected(locShapeCorrected>1)=1;

%identify locations of all domains: voronoi to get local area
[v,c] = voronoin(loc);
for i = 1:length(c),
if all(c{i}~=1) % if at least one of the indices is 1, then it is an open region
locVorArea(i) = polyarea(v(c{i},1),v(c{i},2));
else
locVorArea(i) = 0;
end
end


 a_p = locarea./locperim;
 a_pp = locarea./locperim./locperim;
 bigger = find(a_p>2.8);
 smaller = find(a_p<2.5 & a_p>1);


%Present some results
%figure for Steven's presentation
```

```
   subplot(8,1,2:6);
   imagesc(I(:,:)*10);
   hold on
%   for i = 1:num,
%   bb = props(i).BoundingBox;
%   if find(i==bigger)
%       plot([bb(1), bb(1)+bb(3),bb(1)+bb(3),bb(1),bb(1)], [bb(2), bb(2), bb(2)+bb(4),bb(2)+bb(4),bb
%   elseif find(i==smaller)
%       plot([bb(1), bb(1)+bb(3),bb(1)+bb(3),bb(1),bb(1)], [bb(2), bb(2), bb(2)+bb(4),bb(2)+bb(4),bb
%   else
%       plot([bb(1), bb(1)+bb(3),bb(1)+bb(3),bb(1),bb(1)], [bb(2), bb(2), bb(2)+bb(4),bb(2)+bb(4),bb
%   end
%   end;
   colormap gray
   axis off
   axis equal
   imageaxis = axis;
   linelength_200um = 200/um_per_px;
   rectangle('Position', [50,610/2-10,linelength_200um,20], 'EdgeColor', 'w', 'LineWidth', 4)
   text(50+linelength_200um/2,610/2-10-20, '200um', 'color','w', 'FontSize', 24, 'horizontalalignmen

   subplot(8,1,1);
   barheight = 50;
   numlines = 4; %number of markers+1
   spacing = size(I,2)/numlines;
```

```
   %rectangle('Position', [0.5, 0.5, size(I,2)+0.5, barheight+0.5], 'EdgeColor', 'k', 'LineWidth', 1
   hold on;
   axis off
   axis equal
   axis([0 size(I,2)+1 -barheight/2 barheight+1])
   x=1;
   plot([0.5+x 0.5+x], [0.5-barheight/2 barheight+0.5], 'k', 'LineWidth', 4);

   h1=text(0.5+x+2, 0.5, [strcat(num2str(100*Chol_pixels(round(x)),"%5.1f"),'%') ' Chol.'],'FontSize
   h2=text(0.5+x+2, 0.5+barheight, [strcat(num2str(100*GalCer_pixels(round(x)),"%5.1f"),'%') ' GalCe

   for i = 1:numlines-1,
      x = i*spacing;
      plot([0.5+x 0.5+x], [0.5-barheight/2 0.5], 'k', 'LineWidth', 4);
      text(0.5+x+2, 0.5, strcat(num2str(100*Chol_pixels(round(x)),"%5.1f"),'%'),'FontSize', 16,'vert
      text(0.5+x+2, 0.5+barheight, strcat(num2str(100*GalCer_pixels(round(x)),"%5.1f"),'%'),'FontSiz
   end

   x=size(I,2);
   plot([0.5+x 0.5+x], [0.5-barheight/2 barheight+0.5], 'k', 'LineWidth', 4);
   h1=text(0.5+x-2, 0.5, [strcat(num2str(100*Chol_pixels(round(x)),"%5.1f"),'%')],'FontSize', 16,'ve
   h2=text(0.5+x-2, 0.5+barheight, [strcat(num2str(100*GalCer_pixels(round(x)),"%5.1f"),'%')],'FontS

%area
%   subplot(3,1,3);
%   axis([GalCer_pixels(1) GalCer_pixels(length(GalCer_pixels)) 0 1200]);
%   plot(locgalcer*100, locarea*um_per_px*um_per_px, 'r.', 'MarkerSize', 15);
```

```
%   xlabel('Percentage GalCer','fontsize', 24);
%   ylabel('Domain Area (um^2)','fontsize', 24);
%   set(gca, 'fontsize', 24)
%
%area/perim^2*4pi
%   subplot(3,1,3);
%axis([GalCer_pixels(1) GalCer_pixels(length(GalCer_pixels)) 0 1]);
%   plot(locgalcer*100, locShapeCorrected, 'r.', 'MarkerSize', 15);
%   xlabel('Percentage GalCer','fontsize', 24);
%   ylabel('Area/perim^2*4*\pi','fontsize', 24);
%   set(gca, 'fontsize', 24)

   %area/perim ratio
   subplot(8,1,7:8);
   hold on;
   %axis([GalCer_pixels(1) GalCer_pixels(length(GalCer_pixels)) 0 1]);
   a_p = a_p*um_per_px;
   for i = 1:num,
    if find(i== bigger)
   plot(locgalcer(i)*100, a_p(i), 'r.', 'MarkerSize', 15);
    elseif find(i==smaller)
   plot(locgalcer(i)*100, a_p(i), 'k.', 'MarkerSize', 15);
    else
   %plot(locgalcer(i), a_p(i), 'w.', 'MarkerSize', 8);
    end
   end;
   %x=linspace(.19,.26,1000);
   %usable_high = find(a_p > 2);
```

```
   %area/perim ratio
   subplot(8,1,7:8);
   hold on;
   %axis([GalCer_pixels(1) GalCer_pixels(length(GalCer_pixels)) 0 1]);
   a_p = a_p*um_per_px;
   for i = 1:num,
    if find(i== bigger)
   plot(locgalcer(i)*100, a_p(i), 'r.', 'MarkerSize', 15);
    elseif find(i==smaller)
   plot(locgalcer(i)*100, a_p(i), 'k.', 'MarkerSize', 15);
    else
   %plot(locgalcer(i), a_p(i), 'w.', 'MarkerSize', 8);
    end
   end;
   %x=linspace(.19,.26,1000);
   %usable_high = find(a_p > 2);
   %usable_low = find(a_p < 2 & a_p>1);
   %plot(x, polyval(polyfit(100*locgalcer(usable_high), a_p(usable_high), 4), x));
   %plot(x, polyval(polyfit(100*locgalcer(usable_low), a_p(usable_low), 4), x));
   axis([.19*100 .26*100 0.5 4.5])
   xlabel('% GalCer','fontsize', 24);
   ylabel('Area/perim. (um)','fontsize', 24);
   set(gca, 'fontsize', 24)

   set(gcf, 'position', [478    214    781   1157])
   %set(gcf, 'position', [478   498   811*1.5   873*1.5])
   %screencap
```